# Particle orbits in a force-balanced, wave-driven, rotating torus

I. E. Ochs, and N. J. Fisch

---

**Articles you may be interested in**

Electron holes in phase space: What they are and why they matter
Physics of Plasmas **24**, 055601 (2017); 10.1063/1.4976854

Centrifugal instability in the regime of fast rotation
Physics of Plasmas **24**, 082102 (2017); 10.1063/1.4994546

Toroidal angular momentum balance during rotation changes induced by electron heating modulation in tokamak plasmas
Physics of Plasmas **24**, 080701 (2017); 10.1063/1.4996017

ERO modelling of tungsten erosion and re-deposition in EAST L mode discharges
Physics of Plasmas **24**, 092512 (2017); 10.1063/1.4991457

---

# Particle orbits in a force-balanced, wave-driven, rotating torus

I. E. Ochs[1,2] and N. J. Fisch[1,2]

[1]*Department of Astrophysical Sciences, Princeton University, Princeton, New Jersey 08540, USA*
[2]*Princeton Plasma Physics Laboratory, Princeton, New Jersey 08543, USA*

A wave-driven rotating torus is a recently proposed fusion concept where the rotational transform is provided by the $E \times B$ drift resulting from a minor radial electric field. This field can be produced, for instance, by the RF-wave-mediated extraction of fusion-born alpha particles. In this paper, we discuss how macroscopic force balance, i.e., balance of the thermal hoop force, can be achieved in such a device. We show that this requires the inclusion of a small plasma current and vertical magnetic field and identify the desirable reactor regime through free energy considerations. We then analyze particle orbits in this desirable regime, identifying velocity-space anisotropies in trapped (banana) orbits, resulting from the cancellation of rotational transforms due to the radial electric and poloidal magnetic fields. The potential neoclassical effects of these orbits on the perpendicular conductivity, current drive, and transport are discussed. *Published by AIP Publishing.*
[http://dx.doi.org/10.1063/1.4991510]

## I. INTRODUCTION

In a tokamak or stellarator, the rotational transform necessary for toroidal confinement is produced by the twist in the field lines introduced by the poloidal magnetic field. However, motion along twisted field lines is not the only way to mitigate the vertical drifts which occur in a toroidal magnetic field. For instance, in low-temperature, single-species plasmas often of interest in particle physics,[1] the minor-radial electric field due to space-charge results in a poloidal $E \times B$ drift which offsets the vertical drift.[2] This *magneto-electric confinement* has been demonstrated to confine a cold electron plasma for thousands of poloidal rotation periods.[3]

The potential for magneto-electric confinement in fusion plasmas has been less thoroughly studied. In the early days of the fusion program, T. H. Stix pointed out that fast ion losses near the edge of the plasma could produce a narrow, $E \times B$-rotating region, resulting in confined, D-shaped orbits when combined with the vertical drifts.[4–6] The experiments that seek to manipulate the electric fields in tokamaks via electrodes, such as the electric tokamak at UCLA[7] and the TCABR tokamak[8] at the University of Sao Paulo, have been similarly focused on a thin edge region, where they have often had success in controlling the poloidal flows.[9]

Recently, it has been proposed to replace the poloidal magnetic field entirely with a minor radial electric field,[10] with the requisite volumetric space charge produced by the RF wave-driven extraction of positively charged fusion products.[11,12] This wave-driven extraction is predicted to be more efficient than classical RF-driven current drive in tokamaks.[13,14] In addition, such a confinement system could produce the same rotational transform with less available free energy, suggesting that turbulent transport and instabilities could be reduced compared to the tokamak case.

There are many research questions to be addressed in considering this new confinement scheme, as it is adapted for a multi-species plasma. These include, but are not limited to analyses of MHD and kinetic stability, demonstration that the perpendicular conductivity will allow such a large radial field to be sustained, estimates of the viscous power dissipation due to the poloidal flow, and elucidation of the mechanisms for $\alpha$ particle extraction. In this paper, we leave aside most of these questions for now and only aim to demonstrate that single-particle confinement and macroscopic force balance (i.e., balance of the hoop force) can be simultaneously achieved for a hot fusion plasma.

In the case of cold, single-species, non-neutral plasmas,[1–3] the hoop force was balanced by the electric field from image charges in the conducting wall of the chamber. However, we find (Appendix A) that force balance is likely far more easily achieved in a fusion plasma with a small plasma current and vertical field than with an electric field.

We begin Sec. II by establishing constraints on reactor design, allowing us to identify desirable, macroscopically force-balancing field configurations based on typical fusion plasma pressures. Then, in Sec. III, we analyze particle orbits using constants of motion, showing that we recover known tokamak results in the limit of no electric field, in particular, the trapped, banana-shaped orbits of the neoclassical regime. In Sec. IV, we analyze these orbits in detail for the **wave-driven rotating torus** (WDRT) with purely toroidal flux surfaces, demonstrating how similarly trapped orbits can result from the cancellation of $E \times B$ motion with thermal motion along the small poloidal component of the magnetic field. Interestingly, we find that only electrons are likely to experience these trapped orbits, due to anisotropy of the trapping region in velocity space. In Sec. V, we confirm our analytical results with single-particle simulations and examine the impact of including relativistic effects and vertical fields consistent with force balance, which are minor. Finally, in Sec. VI, we examine the consequences of non-equipotential flux surfaces in a simple field configuration, showing how too large an electric field parallel to the magnetic field can lead to trapped orbits for the entire electron population. The

consequences of our results for the fusion reactor design are discussed in Sec. VII.

## II. DEFINING THE REACTOR REGIME

### A. Constraints on the reactor design

A wave-driven rotating torus has fundamentally different drives and sources of free energy compared to a tokamak, giving rise to different constraints on the system. In this section, we outline these constraints.

The first constraint arises from the fact that an optimal WDRT should be able to almost directly convert $\alpha$ particle birth energy into radial potential energy. Although it is in theory possible to confine the plasma via an electric field pointing in either direction, an inward-pointing field is far more attractive, since fast ions will be cooled as they leave the device, converting their kinetic energy into $E \times B$ rotation. Thus, $\alpha$ particles should lose most of their $\epsilon_\alpha \approx 3.5$ MeV birth energy via direct conversion as they leave the plasma, i.e.,

$$\epsilon_\alpha \approx 2eE_r a, \tag{1}$$

where $E_r$ is the (minor) radial electric field, $e$ is the elementary charge, and $a$ is the minor radius. The coordinate systems used throughout this paper are presented in Fig. 1.

It is also desirable to have sources of free energy in the plasma-sustained fields to be small compared to a conventional tokamak; this is one of the main advantages of the WDRT. For the magnetic field, this is accomplished via the condition $\beta_p \gg 1$, where
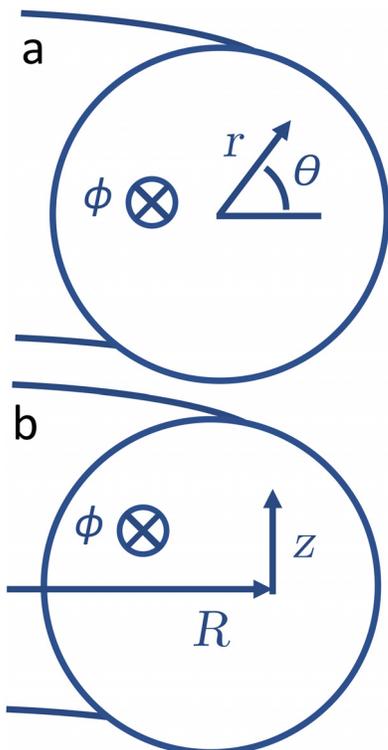


a

b

FIG. 1. Coordinate systems used throughout this paper. We will often find it useful to work in the poloidal coordinates $R$ and $r$, which together implicitly define $\theta$ and $z$ up to a sign.

$$\beta_p = \frac{\int P\,da}{\mu_0 I^2/8\pi} \tag{2}$$

is the ratio between the thermal energy and the pressure in the poloidal magnetic field.

In addition to the poloidal magnetic field, there is also a large radial electric field, which gives rise to two additional sources of free energy, from the electric field itself and from the plasma rotation. Both these are accounted for in the dielectric tensor, so that the energy, and so, the "electric $\beta$" is given by

$$\beta_E \equiv \frac{\langle P \rangle}{\epsilon_0 \langle \epsilon_{rr} E_r^2 \rangle/2}. \tag{3}$$

If $\beta_E \gg 1$, we will also ensure that the hoop force from the electric field pressure is negligible compared to the thermal plasma pressure.

Now because $\hat{r} \perp \hat{b}$, the dielectric tensor component $\epsilon_{rr}$ is given by the low-frequency limit of the Stix $S$ term

$$\epsilon_{rr} = S = 1 + \left(\frac{c}{v_A}\right)^2, \tag{4}$$

where $c/v_A$ is the ratio of the speed of light to the Alfvén ($E \times B$ drift) speed. Since we expect the rotation velocity to be substantially less than the speed of light, most of the energy is stored in the kinetic energy of the $E \times B$ rotation. In this limit, we can express $\beta_E$ straightwardly in terms of the $E \times B$ velocity $v_{E \times B}$

$$\beta_E \approx \frac{\langle P \rangle}{n_i m_i \langle v_{E \times B}^2 \rangle/2}, \tag{5}$$

$$= \frac{\sum_s n_s m_s \langle v_{ths}^2 \rangle}{n_i m_i \langle v_{E \times B}^2 \rangle/2}, \tag{6}$$

$$= (Z_i + 1)\frac{2\langle n_i T \rangle}{m_i \langle n_i v_{E \times B}^2 \rangle}, \tag{7}$$

where we have used $n_e = Z_i n_i$ and assumed $T_i = T_e$. For hydrogen isotopes,

$$\beta_E \sim \left(\frac{2v_{thi}}{v_{E \times B}}\right)^2. \tag{8}$$

Finally, to have minimal shifting of the magnetic axis, so that our flux surfaces approximately enclose our assumed current profile, we want

$$B_{\theta a} > B_z. \tag{9}$$

Our goal will be to combine these constraints with the requirement of macroscopic force balance.

### B. Macroscopic force balance and reactor regime

Macroscopic force balance in a toroidal system requires that we balance the hoop force that causes the plasma to expand, given by

$$F_h = 4\pi \int P da. \tag{10}$$

If a total current $I_\phi$ runs toroidally through the plasma, then this hoop force can be balanced by the addition of a vertical magnetic field

$$B_z = -\frac{2\int P da}{R_0 I_\phi}. \tag{11}$$

This result corresponds to the $\beta_p \to \infty$ limit of the tokamak vertical field at a large aspect ratio[15]

$$B_z = -\frac{\mu_0 I}{4\pi R_0}\left(\log\left(\frac{8R_0}{a}\right) + \Lambda - \frac{1}{2}\right), \tag{12}$$

where

$$\Lambda = \beta_p + \frac{l_i}{2} - 1. \tag{13}$$

### C. Reactor regime

Now that we have related the vertical field to the plasma current, we are almost in a position to define the reactor regime. Note that all terms in the estimates which follow are taken to be positive so that it is only the magnitude of the terms which matters.

We will start by combining the conditions on rotational free energy ($\beta_E \gg 1$) and marginal $\alpha$ confinement [(Eq. (1)]

$$v_{thi} \gg \frac{1}{2}v_{E\times B}, \tag{14}$$

$$\gg \frac{1}{2}\frac{E_r}{B_\phi}, \tag{15}$$

$$\gg \frac{1}{2}\frac{\epsilon_\alpha/2ae}{B_\phi}. \tag{16}$$

This can be rearranged to give an expression for the minor radius

$$a \gg a_0 = \frac{1}{4v_{thi}}\frac{V_\alpha}{B_\phi}, \tag{17}$$

where $V_\alpha$ is the voltage corresponding to the easily extractable $\alpha$ particle birth energy—say 2 MV. Thus, we see that there is a fundamentally minimum minor radius if we want to convert most of the $\alpha$ particle birth energy into electric potential, without having more rotational than thermal energy. Taking $T_i = 10$ keV, we have $v_{thi} \approx 10^6$ m/s, and so, if we take a typical tokamak field of $\sim 5$ T, we find $a_0 \approx 10$ cm. Note that $\beta_E \sim (a/a_0)^2$, which means that at a minor radius of about 30 cm, we would have $\beta_E \approx 10$. Thus, quite small sources of free energy seem to be consistent with reasonable device dimensions.

Now, we must impose our force balance condition. For simplicity, we will assume a constant current profile. We start by expressing the magnetic fields in terms of $\beta_p$, subject

to force balance. For the poloidal magnetic field, this is straightforward. First, we define

$$I_0 \equiv \sqrt{\frac{\int P da}{\mu_0/8\pi}} = \sqrt{\frac{8\pi^2\langle P\rangle a^2}{\mu_0}} \tag{18}$$

so that when $I = I_0$, $\beta_p = 1$, and in general, $\beta_p = \left(\frac{I_0}{I}\right)^2$. Then, we have, assuming a constant current profile,

$$B_{\theta a} = \frac{\mu_0 I}{2\pi a} = \frac{\mu_0 I_0}{2\pi a}\beta_p^{-1/2} = \sqrt{\frac{2\mu_0\langle P\rangle}{\beta_p}}. \tag{19}$$

The vertical field is then obtained from the force balance condition [(Eq. (11)]

$$B_z \approx \frac{2\int P da}{R_0 I} = \frac{2\pi a^2\langle P\rangle}{R_0 I_0 \beta_p^{-1/2}} = \frac{a}{R_0}\sqrt{\frac{\mu_0\langle P\rangle\beta_p}{2}}. \tag{20}$$

Finally, we include our last constraint that $B_{\theta a} > B_z$, which gives

$$\beta_p < 2\left(\frac{R}{a}\right). \tag{21}$$

Since we need large $\beta_p$, this indicates that the favorable reactor regime lies at a large aspect ratio. However, since we wish to minimize viscous damping of the poloidal rotation, the large aspect ratio was the regime of interest anyway.

It is instructive to consider the requisite fields for typical fusion temperatures and densities. First, note that the pressure is given by

$$P = \sum_s n_s T_s = 1.6 \times 10^4 \sum_s n_{s,20} T_{s,\text{keV}}, \tag{22}$$

where $n_{s,20}$ is the density of species $s$ normalized to $10^{20}$ m$^{-3}$ and $T_{s,\text{keV}}$ is the temperature of species $s$ in keV. If we additionally assume parabolic profiles $n, T \sim 1 - (r/a)^2$, then

$$\langle P\rangle = \frac{\int_0^a P_{\max}\left(1 - \left(\frac{r}{a}\right)^2\right)2\pi r dr}{\pi a^2} = \frac{1}{3}P_{\max}. \tag{23}$$

Thus,

$$\langle P\rangle = 5.3 \times 10^3 \sum_s n_{s,20} T_{s,\text{keV}}. \tag{24}$$

With these assumptions and additionally assuming $T_{i,\text{keV}} = T_{e,\text{keV}} = T_{\text{keV}}$, $n_{e,20} = n_{20}$, we can write the fields in SI as

$$B_{\theta a} = 0.12\sqrt{\frac{(Z_i^{-1} + 1)n_{20}T_{keV}}{\beta_p}}. \tag{25}$$

$$B_z = 0.058\frac{a}{R}\sqrt{(Z_i^{-1} + 1)n_{20}T_{keV}\beta_p}. \tag{26}$$

For a reactor with a major radius of 10 m and a minor radius of 30 cm, confining a $T = 10$ keV, $n_e = 5 \times 10^{19}$ m$^{-3}$ D-T

plasma at a $\beta_p$ value of 10, we thus have $B_{\theta a} = 0.12$ T and $B_z = 0.017$ T.

## III. PARTICLE ORBITS

Now that we have a rough picture of how to introduce macroscopic force balance in a WDRT, we will re-examine particle trajectories with the consistent poloidal and vertical fields for force balance. We will assume that there is infinite conductivity parallel to the magnetic field so that flux surfaces are equipotentials.

Our constants of motion are then

$$\epsilon = \frac{1}{2}mv_\perp^2 + \frac{1}{2}mv_\parallel^2 + qV(\Phi), \tag{27}$$

$$\mu = \frac{1}{2}\frac{mv_\perp^2}{|B|}, \tag{28}$$

$$p_\phi = mRv_\phi + q\Phi. \tag{29}$$

Eliminating the final velocities using the last two equations and taking $v_\parallel = |B|/B_\phi v_\phi$, we thus have the orbit constraint equation

$$0 = \frac{1}{2}m\left(\frac{|B|}{|B_i|} - 1\right)v_{\perp i}^2 + \frac{1}{2}\left[\left(\frac{R_i}{R}v_{\phi i}^2 - \frac{q}{mR}\Delta\Phi\right)^2\frac{|B|^2}{B_\phi^2} - v_{\phi i}^2\frac{|B_i|^2}{B_{\phi i}^2}\right] + q(V(\Phi) - V(\Phi_i)), \tag{30}$$

where we have defined $\Delta\Phi = \Phi - \Phi_i$.

Now we make a couple of approximations, based on the assumption that the particle will not deviate far from the flux surface. The first consequence of this is that the relative strength of the poloidal and toroidal fields should not change dramatically; thus, we take $\frac{|B_i|^2}{B_{\phi i}^2} \approx \frac{|B|^2}{B_\phi^2}$.

The second consequence is that we can Taylor expand the potential around the flux surface, i.e.

$$V(\Phi) - V(\Phi_i) \approx \frac{\partial V}{\partial\Phi}\Delta\Phi. \tag{31}$$

Here, we assume that $\Delta\Phi$ is not large enough that $\frac{\partial V}{\partial\Phi}$ changes significantly.

Now, we will define a few ratios

$$\hat{R}_i \equiv \frac{R_i}{R}, \tag{32}$$

$$\chi_M \equiv \frac{|B|}{|B_i|} - 1, \tag{33}$$

$$\chi_C \equiv \hat{R}_i^2 - 1, \tag{34}$$

$$\chi_\alpha \equiv \frac{|B_i|^2}{B_{\phi i}^2}. \tag{35}$$

The first of these terms simply relates the current and initial major radii; the second involves the mirror force, the third is a centrifugal term, and the fourth involves the pitch angle of the magnetic field. It should be noted that

$$v_{\parallel i}^2 = v_{\phi i}^2\chi_\alpha. \tag{36}$$

The orbit constraint equation can then be written in terms of these variables

$$0 = A(\Delta\Phi)^2 + B\Delta\Phi + C, \tag{37}$$

where

$$A = \frac{q^2}{2mR^2}\chi_\alpha, \tag{38}$$

$$B = -q\frac{R_iv_{\phi i}}{R^2}\chi_\alpha + q\frac{\partial V}{\partial\Phi}, \tag{39}$$

$$C = \frac{1}{2}m\chi_Mv_{\perp i}^2 + \frac{1}{2}m\chi_C\chi_\alpha v_{\phi i}^2. \tag{40}$$

The solution is, of course,

$$\Delta\Phi = -\frac{B}{2A}\left(1 \pm \sqrt{1 - \frac{4AC}{B^2}}\right). \tag{41}$$

Now, much of the useful physics is contained in

$$D \equiv \frac{4AC}{B^2} = \frac{\chi_\alpha\left(\chi_Mv_{\perp i}^2 + \chi_Cv_{\parallel i}^2\right)}{\left(R\frac{\partial V}{\partial\Phi} - \hat{R}_iv_{\phi i}\chi_\alpha\right)^2}. \tag{42}$$

Typically, this will be small since $\chi_M, \chi_C \ll 1$. In this case, we can Taylor expand to find $\Delta\Phi$. The exception will be when the denominator goes to zero with a finite numerator, in which case we can expect trapped (banana) orbits.

### A. Verification of Tokamak trapping

To show that the limit $D > 1$ corresponds to tokamak trapping, we will first consider $\frac{\partial V}{\partial\Phi} = 0$, which describes a large-aspect-ratio tokamak, and show that we recover the banana orbit condition. We will then extend these results to large $E_r$ in Secs. IV and V.

If we let $\frac{\partial V}{\partial\Phi} \to 0$, then we simply have a (non-inductively-driven) tokamak. Then, our condition for particle trapping becomes

$$1 < D = \frac{\chi_\alpha\left(\chi_Mv_{\perp i}^2 + \chi_Cv_{\parallel i}^2\right)}{\left(\hat{R}_iv_{\phi i}\chi_\alpha\right)^2} = \frac{\chi_Mv_{\perp i}^2 + \chi_Cv_{\parallel i}^2}{\hat{R}_i^2v_{\parallel i}}, \tag{43}$$

i.e.,

$$v_{\parallel i}^2 < \chi_Mv_{\perp i}^2 = \left(\frac{|B|}{|B_i|} - 1\right)v_{\perp i}^2. \tag{44}$$

We can recognize this as the mirror trapping condition.[15,16]

### IV. TRAPPED ORBITS IN WDRT

Once the electric field is added, the denominator of $D$ contains two terms and the trapping condition becomes (in part) a resonance condition. The center and width of this resonance will determine how much of the particle population

lives on trapped orbits. However, first, we must have an explicit form for $\frac{\partial V}{\partial \Phi}$.

## A. Field setup

For simplicity, we take $B_z$ constant, and

$$B_\theta = \left(\frac{R_0}{R}\right)\left(\frac{r}{a}\right)B_{\theta a}, \tag{45}$$

where $R$ is the major radial coordinate, $R_0$ is the center of the magnetic axis, $r$ is the minor radial coordinate, and $a$ is the plasma minor radius at $\theta = \pi/2$. Then, our flux function $\Phi = RA_\phi$ is given by

$$\Phi = \frac{1}{2}R^2 B_z + \frac{1}{2}R_0 \frac{r^2}{a}B_{\theta a}. \tag{46}$$

As we show in Appendix B, this choice of $B_\theta$ gives us concentric flux surfaces centered around

$$R_v \equiv R_0\left(1 + \frac{a}{R_0}\frac{B_z}{B_{\theta a}}\right)^{-1}. \tag{47}$$

By taking the electric field to be constant at $R = R_v$, it is also found that

$$\frac{\partial V}{\partial \Phi} = -E_r\left(\frac{a}{R_0 z_v B_{\theta a}}\right), \tag{48}$$

where $z_v(\Phi)$ is the height of the flux surface $\Phi$ at $R = R_v$ (Fig. 2).

## B. Resonance center for trapped orbits

To better understand the resonance condition, take $B_z = 0$, so that

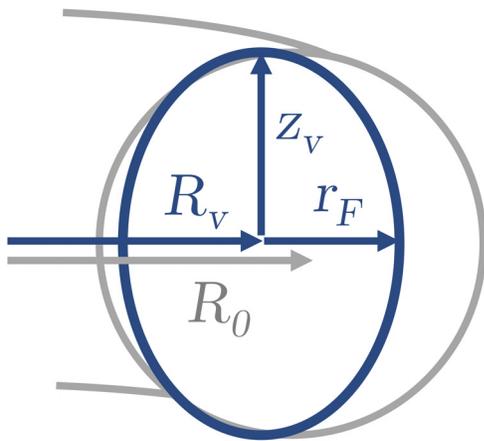$$\Phi = \frac{1}{2}R_0 \frac{r^2}{a}B_{\theta a}. \tag{49}$$



FIG. 2. Elongation and shift of flux surfaces and associated coordinates at finite $B_z$. As $B_z$ increases, the flux surface center $R_v$ shifts inward from the poloidal origin at $R_0$, and the flux surface elongates vertically. Throughout this paper, we take the minor radius of the device $a$ to correspond to the highest vertical extent $z_v$ of the outer flux surface. We also define a radial coordinate $r_F$ which is measured from the center of the flux surface rather than from the center of our toroidal coordinate system.

Then, $z_v = r$, and Eq. (48) becomes

$$\frac{\partial V}{\partial \Phi} = -E_r \frac{a}{rR_0 B_{\theta a}}. \tag{50}$$

Now, the particle will start moving across many flux surfaces when the denominator of $D$ is 0. Setting the denominator of Eq. (42) to 0, we have

$$0 = \hat{R}_i v_{\phi i}\chi_\alpha - R\frac{\partial V}{\partial \Phi}, \tag{51}$$

$$= \hat{R}_i v_{\phi i}\chi_\alpha + RE_r\frac{a}{rR_0 B_{\theta a}}, \tag{52}$$

$$= \hat{R}_i v_{\phi i}\chi_\alpha + \frac{E_r}{B_\theta}, \tag{53}$$

where in the last line we made use of the definition of $B_\theta$.

Now, we multiply the last line by $\frac{B_\phi B_\theta}{|B|^2}$ and also recall the definition of $\chi_\alpha \equiv \frac{|B_i|^2}{B_{\phi i}^2}$. Then, we have

$$0 = v_\parallel \Pi_{\hat{B},\hat{\theta}} + v_{E\times B}\Pi_{\hat{r}\times\hat{B},\hat{\theta}}, \tag{54}$$

where

$$v_\parallel \equiv \hat{R}_i v_{\parallel i} \tag{55}$$

is the parallel velocity consistent with momentum conservation *if the particle remains on its initial flux surface*, and

$$\Pi_{\hat{B},\hat{\theta}} \equiv \frac{B_\theta}{|B|}, \tag{56}$$

$$\Pi_{\hat{r}\times\hat{B},\hat{\theta}} \equiv \frac{B_\phi}{|B|} \tag{57}$$

are operators which project the parallel and $E \times B$ velocities onto $\hat{\theta}$, respectively.

Thus, we can see that the particle moves across many flux surfaces when the rotational transforms due to velocity along the field line and $E \times B$ drift across the field line cancel. We can summarize this condition as $v_{\theta,RT} = 0$, where

$$v_{\theta,RT} \equiv v_\parallel \Pi_{\hat{B},\hat{\theta}} + v_{E\times B}\Pi_{\hat{r}\times\hat{B},\hat{\theta}}. \tag{58}$$

It is worth noting that in the case where $E_r$ points inward, which is the case of interest for the WDRT, electrons which support the plasma current are more likely to be trapped; thus, there could be an enhanced resistivity even beyond the normal neoclassical term.

It is worth noting that trapped partical effects are not necessarily deleterious. For instance, absorption of Alfven waves by trapped particles has been shown to produce sheared poloidal rotation,[17] which is important in the formation of transport barriers for accessing the H-mode.

## C. Resonance width

The boundaries of the resonance are given by $D = 1$. The following analysis will become simpler with the following normalized definitions:

$$\hat{\Pi} \equiv \frac{\Pi_{\hat{r} \times \hat{B}, \hat{\theta}}}{\Pi_{\hat{B}, \hat{\theta}}} = \frac{B_\phi}{B_\theta}, \tag{59}$$

$$\hat{v}_{\|i} \equiv \frac{v_{\|i}}{v_{E \times B}}, \tag{60}$$

$$\hat{v}_{\perp i} \equiv \frac{v_{\perp i}}{v_{E \times B}}. \tag{61}$$

Note that $v_{E \times B} > 0$ if $E_r > 0$ and $v_{E \times B} < 0$ if $E_r < 0$. In general, we will also have $\hat{\Pi} \gg 1$.

In these new variables, our resonance boundaries are given by

$$D = \frac{\chi_C \hat{v}_{\|i}^2 + \chi_M \hat{v}_{\perp i}^2}{(\hat{v}_{\|i} \hat{R}_i + \hat{\Pi})^2} = 1. \tag{62}$$

When we solve this for $\hat{v}_{\|i}$, we find

$$\hat{v}_{\|i} = -\hat{R}_i \hat{\Pi} \pm \sqrt{\chi_C \hat{\Pi}^2 + \chi_M \hat{v}_{\perp i}^2}. \tag{63}$$

Thus, the trapping region is defined by a hyperbola in velocity space

$$\left( \hat{v}_{\|i} + \hat{R}_i \hat{\Pi} \right)^2 - \chi_M \hat{v}_{\perp i}^2 < \chi_C \hat{\Pi}^2. \tag{64}$$

Interestingly, a similarly shaped trapping region was calculated for impurities in a toroidally rotating plasma, where it resulted from the inclusion of the Coriolis force.[18]

Now, our relatively small poloidal field ensures $\hat{\Pi} \gg 1$, while $v_{E \times B}$ is some large fraction of the ion thermal velocity. Our resonant trapped velocity will thus be much larger than the ion thermal velocity, making ion trapping rare. Thus, we only expect a significant number of trapped orbits for electrons in the WDRT, as well as potentially for fusion-born $\alpha$ particles.

### D. Banana width

To find the banana width, let the discriminant in Eq. (41) be 0. Then

$$\Delta\Phi = -\frac{B}{2A}, \tag{65}$$

$$= \frac{mR}{q} \left( \frac{B_\phi}{B_\theta} \right) v_{\theta, RT}. \tag{66}$$

Now, we make use of the approximation

$$\Delta\Phi = RB_\theta \Lambda \tag{67}$$

which gives

$$\Lambda = \frac{1}{\Omega_p} \hat{\Pi} v_{\theta, RT}, \tag{68}$$

where $\Omega_p = qB_\theta/m$.

The "fattest banana" is generally the most marginally trapped orbit, given from inequality (64) by

$$v_{\theta, RT}^2 \approx \chi_M v_{\perp i}^2 \Pi_{\hat{B}, \hat{\theta}}^2 + \chi_C v_{E \times B}^2 \Pi_{\hat{r} \times \hat{B}, \hat{\theta}}^2. \tag{69}$$

So, substituting this in above, we get

$$\Lambda = \left( \sqrt{\chi_M} \frac{v_\perp}{\Omega_p} \right) \Pi_{\hat{r} \times \hat{B}, \hat{\theta}} \sqrt{1 + \frac{\chi_C}{\chi_M} \frac{\hat{\Pi}^2}{\hat{v}_{\perp i}^2}}. \tag{70}$$

The first part, in parentheses, is the conventional banana width. In general, for electrons, we will have $v_{the} \gg v_{E \times B}$, and so, the denominator of the second term in the square root should be large–on the order of an electron-ion mass ratio. However, the numerator is determined by $\hat{\Pi} = B_\phi/B_\theta \gg 1$, and so, it is easy to envision this being the dominant term. In that case, the banana scaling will be given by (assuming $\Pi_{\hat{r} \times \hat{B}, \hat{\theta}} \approx 1$)

$$\Lambda = \sqrt{\chi_C} \frac{v_{E \times B}}{\Omega_p} \frac{B_\phi}{B_\theta} = \sqrt{\chi_C} \frac{1}{\Omega_p} \frac{E_r}{B_\theta}. \tag{71}$$

Assuming $\chi_C \approx \chi_M$ means that the main difference is that we replace the thermal velocity with

$$v_{E \times B_\theta} \equiv \frac{E_r}{B_\theta} \tag{72}$$

when calculating the banana widths.

### E. Large aspect ratio

For the purpose of clarity and easy comparison to the transport literature, it is instructive to take the large-aspect ratio limit of our results. In a large-aspect-ratio WDRT, we will have

$$\chi_M \sim \frac{R + a}{R - a} - 1 \approx 2\varepsilon, \tag{73}$$

$$\chi_C \sim \frac{(R + a)^2}{(R - a)^2} - 1 \approx 4\varepsilon. \tag{74}$$

Here, we have adopted the convention from the neoclassical transport literature, denoting the inverse aspect ratio $\varepsilon \equiv a/R$.

Our trapping region is given at a large aspect ratio from Eq. (64) by

$$\left( \hat{v}_{\|i} + \hat{\Pi} \right)^2 - 2\epsilon \hat{v}_{\perp i}^2 < 4\epsilon \hat{\Pi}^2. \tag{75}$$

Or, more dimensionally

$$\left( v_{\|i} + v_{E \times B} \frac{B_\phi}{B_\theta} \right)^2 < 2\epsilon v_{\perp i}^2 (1 + 2\xi), \tag{76}$$

where

$$\xi \equiv \left( \frac{v_{E \times B}}{v_{\perp i}} \right)^2 \left( \frac{B_\phi}{B_\theta} \right)^2 \tag{77}$$

is the critical parameter which determines the degree of deviation from tokamak-type trapping. In a WDRT, $\xi \gg 1$.

TABLE I. Sample reactor parameters for a force-balancing WDRT scenario, confining a $T = 10\,\text{keV}$, $n_e = 5 \times 10^{19}\,\text{m}^{-3}$ D-T plasma.

| Parameter | Value |
|---|---|
| $a$ | 0.3 m |
| $R_0$ | 10 m |
| $\varepsilon$ | 0.03 |
| $E_r$ | $3 \times 10^6$ V/m |
| $B_\phi$ | 5.0 T |
| $B_\theta$ | 0.1 T |
| $B_z$ | 0.02 T |
| $v_{E\times B}$ | $6 \times 10^5$ m/s |
| $v_{thi}$ | $1 \times 10^6$ m/s |
| $v_{the}$ | $4 \times 10^7$ m/s |
| $\beta_p$ | 10 |
| $\beta_E$ | 10 |

Thus, compared to the tokamak case, the trapping region both shifts and expands, with the degree of each determined by both the ratio of $v_{E\times B}$ to $v_{the}$, and $B_\theta$ to $B_\phi$. Unlike in tokamak banana transport, the toroidal field plays a role in determining the shape of the trapping region.

In its two limits

$$\left(v_{\|i} + v_{E\times B}\frac{B_\phi}{B_\theta}\right)^2 < \begin{cases} 2\epsilon v_{\perp i}^2 & \text{if } \xi \ll 1 \\ 4\epsilon v_{E\times B}^2 \left(\frac{B_\phi}{B_\theta}\right)^2 & \text{if } \xi \gg 1. \end{cases} \tag{78}$$

Once the trapping region is known, the fattest banana width is given by

$$\Lambda = \left(\sqrt{2\epsilon}\frac{v_\perp}{\Omega_p}\right)\sqrt{1 + 2\frac{\hat{\Pi}^2}{\hat{v}_{\perp i}^2}}. \tag{79}$$

Or, more dimensionally

$$\Lambda = \left(\sqrt{2\epsilon}\frac{v_\perp}{\Omega_p}\right)\sqrt{1 + 2\xi}. \tag{80}$$

In its two limits

$$\Lambda = \begin{cases} \sqrt{2\epsilon}\dfrac{v_\perp}{\Omega_p} & \text{if } \xi \ll 1 \\ \sqrt{4\epsilon}\dfrac{1}{\Omega_p}\dfrac{E_r}{B_\theta} & \text{if } \xi \gg 1. \end{cases} \tag{81}$$

In contrast to the shape of the trapping region [Eq. (76)], the banana width is always independent of the toroidal field.

For the values in Table I, the electron fattest banana width is on the order of 1 mm. Thus, assuming banana diffusion, trapping should not lead to any sudden loss of confinement due to instantaneously lost orbits although it could lead to enhanced conductivity perpendicular to the magnetic field.

## V. SIMULATIONS AND FINITE $B_z$

To test our analytical predictions, we performed single-particle full-orbit simulations for the device parameters shown in Table I using either a non-relativistic Boris[19] or relativistic Vay[20] particle pusher and the field configuration described in Appendix B. Particles were initialized on the low-field side of the outer flux surface at $z = 0$, as described in Appendix B 1. To map the trapped region in phase space, the initial velocity was swept across a range of initial values $v_{\perp i}$ and $v_{\|i}$ in the approximate $E \times B$-drifting rest frame; i.e., the particle with $(v_{\perp i} = 0, v_{\|i} = 0)$ was initialized at $\mathbf{v}_i = \frac{\mathbf{E} \times \mathbf{B}}{B^2}$.

Simulation results for the trapping region for $B_z = 0$ are shown in Fig. 3 for both particle pushers. The trapping region is well described by the analysis and is largely unaffected when relativistic effects are included.

When we add a finite $B_z$ that ensures macroscopic force balance (0.021 T for the parameters in Table I), the trapping region is largely unaffected, but the banana orbits get slightly wider, especially at low $v_{\perp i}$ (Figs. 4 and 5). Thus, macroscopic force balance in a WDRT with equipotential flux surfaces seems to be fairly achievable from a single-particle perspective.

Finally, an example of a simulated trapped electron orbit is shown in Fig. 6. Apart from the finite banana width at negligible initial $v_{\perp i}$, the orbits are clearly similar to the banana-trapped orbits in a tokamak, of which they are a generalization.

## VI. NON-EQUIPOTENTIAL FLUX SURFACES

The extremely high $q$ (low $B_\theta$) anticipated for the WDRT means that an electron must traverse a large distance along a field line in order to traverse a short distance poloidally. Thus, it is not trivially guaranteed that the flux
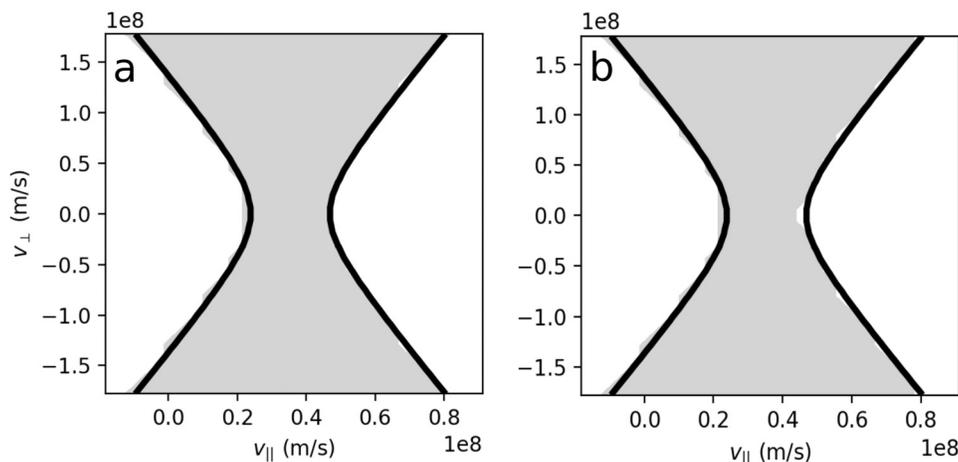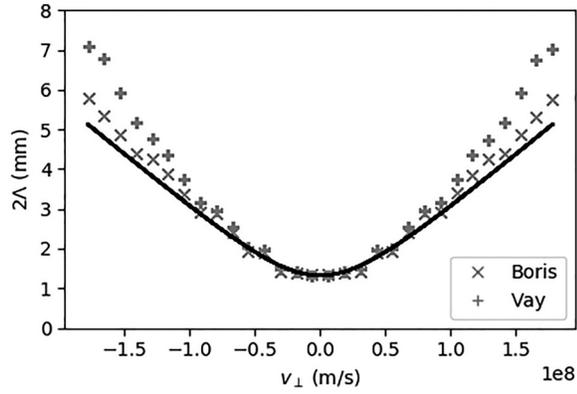


FIG. 3. Simulated trapped orbit region (gray) using non-relativistic Boris (a) relativistic Vay and (b) particle pushers. Analytical results from Eq. (64) are given in black.

FIG. 4. Fattest full banana width across $v_{\|i}$ as a function of $v_{\perp i}$ using non-relativistic Boris and relativistic Vay particle pushers. Analytical results from Eq. (80) are given in black. As $v$ becomes significant compared to the speed of light, the trapped orbits grow wider, consistent with the increasing relativistic mass.

surfaces will be equipotential, and it is worth considering the consequences of non-equipotential flux surfaces.

As a simple model for this situation, consider that we have the same flux function $\Phi$ as in Eq. (46), but now we have an electric field $\mathbf{E} = E_r \hat{r}$ that points purely radially. Taylor expanding Eq. (47), we see that this will offset the flux surface center from the electric center by a distance

$$\Delta_{cen} \equiv R_v - R_0 \approx -a \frac{B_z}{B_{\theta a}}. \tag{82}$$

If we carry out the same constants of motion analysis for this situation, then we find that wide, trapped orbits will result even for cold particles unless (in the limit $B_{\theta a} \gg B_z$)

$$|E_r| > 4 \frac{e}{m} B_z B_{\theta a} a. \tag{83}$$

In contrast to the equipotential flux surface case, the resulting trapped orbits can occur on either the high- or low-field side of the device. For a derivation of this result from the constants of motion, see Appendix C.
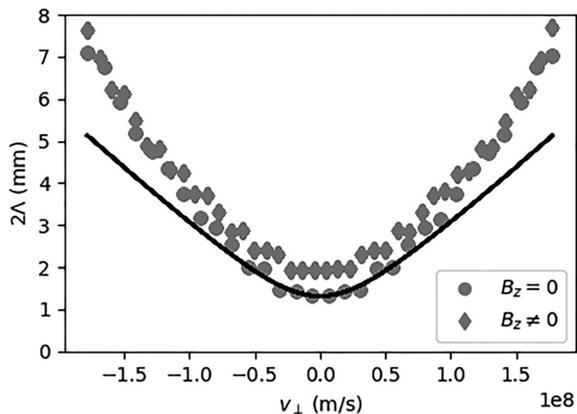


FIG. 5. Fattest full banana width across $v_{\|i}$ as a function of $v_{\perp i}$ without a vertical magnetic field and with a macroscopic force-balancing vertical field of 0.021 T, using the Vay relativistic pusher. Analytical results from Eq. (80) are given in black. The vertical field does not have much effect on the banana width although it has a moderate impact at low $v_{\perp i}$ in increasing the banana width.
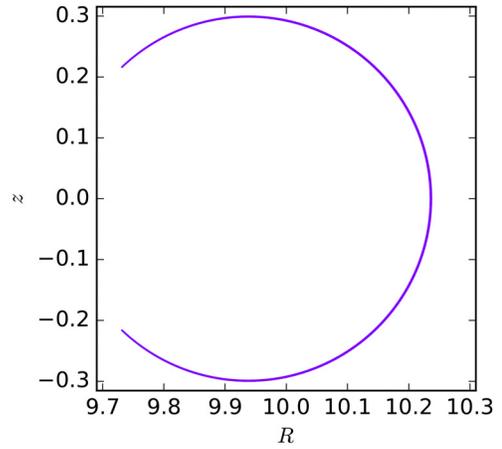


FIG. 6. Poloidal projection of the trapped electron orbit for configuration with finite $B_z$. This electron was initialized with $v_{\|i} = 4.6 \times 10^7$ m/s and $v_{\perp i} = 0$ at $r = a$ on the outboard side, resulting in a banana width of 1.8 mm. The inward shift of the flux surface center by about 6 cm due to $B_z$ (see Appendix B) is visible in the center of the orbit.

The trapping condition can be understood heuristically as follows. For cold electrons, the rotational transform is provided entirely by the $E \times B$ rotation, and so, an electron at radius $a$ traverses from the high-field to low-field side of the device on a timescale

$$\tau_{E \times B} = \frac{B_\phi}{E_r} \pi a. \tag{84}$$

As the electron traverses this orbit, there is a component of $E_r$ parallel to the magnetic field due to $B_z$. The force along the field line due to the radial $E$ field when $B_z, B_{\theta a} \ll B_\phi$ is thus

$$F_\| = -e E_r \frac{B_z}{B_\phi} \sin \theta. \tag{85}$$

Over the half orbit, the electron thus gains a velocity parallel to the magnetic field

$$v_\| = \frac{F_\|}{m} \tau_{E \times B}. \tag{86}$$

If the projection of this velocity onto $\hat{\theta}$, i.e., $v_\theta = v_\| \frac{B_\theta}{B_\phi}$, is opposite in sign and larger in magnitude than the $E \times B$ velocity, then the electron will reverse the direction, becoming trapped. The rotational transforms will oppose, for instance, for electrons when $E_r < 0$ and $B_z, B_{\theta a} > 0$. Then, the condition for trapping is

$$\frac{E_r}{B_\phi} < v_\theta = \frac{F_\|}{m} \tau_{E \times B} \frac{B_\theta}{B_\phi}. \tag{87}$$

Multiplying by $B_\phi$ and taking $\langle \sin \theta \rangle = \frac{2}{\pi}$, we have

$$E_r < 2 \frac{e}{m} B_z B_\theta a \tag{88}$$

which is within a factor of two of our exact condition from COM.

We can rewrite Eq. (83) in terms of the flux surface shift

$$|E_r| > 4 \frac{e}{m} B_{\theta a}^2 |\Delta_{cen}|. \tag{89}$$

Thus, we see that the condition for passing cold-electron orbits introduces a maximum allowable deviation from equipotential flux surfaces.

## VII. CONCLUSION

We demonstrated via a constants-of-motion approach that fusion-pressure electrons and ions can be well confined in a macroscopically force-balancing wave-driven rotating torus (WDRT) configuration. By so doing, we identified several possible sources of difficulty for the WDRT, which require further research.

Most of these potential problems arise from the fact that the banana-trapping region is not symmetric in phase space along $v_\parallel$. The first consequence of this asymmetry is the trapping of only electrons but not of ions. This differential confinement could have large effects on the perpendicular conductivity, which must be low to sustain the MV-scale potentials needed for the efficient direct conversion of $\alpha$-particle energy.

The second consequence of the asymmetry is the preferential trapping of electrons which support the plasma current, thus potentially increasing the resistivity in excess of the standard neoclassical increase due to symmetric electron trapping. This effect could lower the current drive efficiency.

Finally, we showed that the deviation of flux surfaces from equipotential surfaces could lead to large-scale trapping of the electron population, emphasizing the importance of having large parallel conductivity despite the low perpendicular conductivity.

By confirming that a small toroidal current can lead to a force-balanced plasma, without destroying the WDRT confinement, our results demonstrate the potential promise of the WDRT as a fusion concept with far lower free energy than a tokamak. However, the interesting trapped orbit effects are uncovered as a result also point to the important research avenues ahead in evaluating their feasibility.

## ACKNOWLEDGMENTS

## APPENDIX A: FORCE BALANCE WITH AN ELECTRIC FIELD

It could also be possible to balance the hoop force with an electric field, given the plasma space charge necessary to produce the radial electric field. The size of this space charge can be approximated from Gauss' law, by assuming a cylindrical plasma

$$\epsilon_0 \int E \cdot dA = \int \rho dV = Q_{\text{enc}}. \tag{A1}$$

Solving for a linear charge density $\lambda$, this becomes

$$\lambda = 2\pi r \epsilon_0 E_r. \tag{A2}$$

We now need to produce a force per unit length equal to the force provided by the vertical field above. Thus,

$$F = E_R \lambda = IB_v = -\frac{2 \int P da}{R_0} \tag{A3}$$

which, substituting in $\lambda$, gives

$$E_R = -\frac{\int P da}{\pi r R_0 \epsilon_0 E_r} = 3.6 \times 10^{10} \frac{\int P da}{r R_0 E_r}. \tag{A4}$$

Now, substituting in $\langle P \rangle = 5 \times 10^3 n_{20} T_{\text{keV}}$, then

$$E_R = 5.6 \times 10^{14} \frac{a n_{20} T_{\text{keV}}}{R_0 E_r}. \tag{A5}$$

Combining this with our constraint on marginal alpha confinement [Eq. (1)]

$$E_R = 5.6 \times 10^8 \frac{a}{R_0} n_{20} T_{\text{keV}} a, \tag{A6}$$

where all lengths are measured in meters. Now, in order for $E_R \ll E_r$ (a condition for closed poloidal orbits), we can see that we will have to push to a very large aspect ratio and small $a$; i.e., for $a = 0.3$, we would need $R_0 \gg 100$ m.

This requirement for an extremely large aspect ratio becomes clear when we note that that Eq. (A4) can be written as

$$\frac{E_R}{E_r} = \frac{2a}{R_0} \epsilon_{rr} \frac{\langle P \rangle}{\epsilon_0 \epsilon_{rr} E_r^2 / 2} \approx \frac{2a}{R_0} \left(\frac{c}{v_A}\right)^2 \beta_E, \tag{A7}$$

where $\beta_E$ is defined in Eq. (3) as the ratio of the thermal to electric field energy. Thus, with the rotational energy small compared to the thermal energy (one of the weaker of our free energy constraints), we must go to extremely large aspect ratio. This difficulty makes electrostatic force balance an unattractive option.

## APPENDIX B: ELECTRIC FIELD FOR EQUIPOTENTIAL FLUX SURFACES

For $B_\theta = B_{\theta a} \left(\frac{r}{a}\right)^p \frac{R_0}{R}$, our vector potential is given by

$$A_\phi(R, r) = \frac{1}{2} R B_z + \frac{1}{p+1} \frac{R_0}{R} \frac{r^{p+1}}{a^p} B_{\theta a}, \tag{B1}$$

where $r = \sqrt{(R - R_0)^2 + z^2}$. Thus, our flux $\Phi = RA_\phi$ is given by

$$\Phi = \frac{1}{2} R^2 B_z + \frac{1}{p+1} R_0 \frac{r^{p+1}}{a^p} B_{\theta a}. \tag{B2}$$

The gradient of this, along which the poloidal projection of the electric field will point, is given by

$$\nabla \Phi = \left[ RB_z + R_0 \left( (R - R_0)^2 + z^2 \right)^{\frac{p-1}{2}} \frac{R - R_0}{a^p} B_{\theta a} \right] \hat{R}$$
$$+ \left[ R_0 \left( (R - R_0)^2 + z^2 \right)^{\frac{p-1}{2}} \frac{z}{a^p} B_{\theta a} \right] \hat{z}. \tag{B3}$$

For $p = 1$, corresponding to constant current density and linearly increasing $B_\theta$,

$$\Phi = \frac{1}{2} R^2 B_z + \frac{1}{2} R_0 \left( \frac{(R - R_0)^2 + z^2}{a} \right) B_{\theta a}, \tag{B4}$$

$$\nabla \Phi = \left[ RB_z + R_0 \left( \frac{R - R_0}{a} \right) B_{\theta a} \right] \hat{R} + \left[ R_0 \left( \frac{z}{a} \right) B_{\theta a} \right] \hat{z}. \tag{B5}$$

Note that as $B_z \to 0$, the gradient points purely along $\hat{r} = \cos \theta \hat{R} + \sin \theta \hat{z}$.

Now, in general, the constant-flux surfaces will be elongated along $\hat{z}$ and compressed along $\hat{R}$. They will also no longer be centered around $R = R_0$. Instead, we can easily identify the point at which $\nabla \Phi$ points purely vertically from Eq. (B5). Setting the $\hat{R}$ term to 0, we find that this occurs at $R = R_v$, where

$$R_v = R_0 \left( 1 + \frac{a}{R_0} \frac{B_z}{B_{\theta a}} \right)^{-1}. \tag{B6}$$

Now, we choose to define our $E$ field profile along this line where $\nabla \Phi$ is vertical. We will call the field along this line $E_r(z_v(\Phi))$, where $z_v(\Phi)$ is the unique positive value of $z$ where a given flux surface $\Phi$ intersects this line. We can find $z_v(\Phi)$ simply by plugging $R = R_v$ into Eq. (B4) and solving for $z_v$. This gives

$$z_v = \sqrt{ \frac{2a}{R_0 B_{\theta a}} \left( \Phi - \frac{1}{2} R_v^2 B_z \right) - (R_v - R_0)^2 }. \tag{B7}$$

Now

$$\mathbf{E} = -\nabla V = -\frac{\partial V}{\partial \Phi} \nabla \Phi. \tag{B8}$$

At $R = R_v$, $\nabla \Phi \parallel \hat{z}$, and this becomes

$$E_r(z_v) = -\frac{\partial V}{\partial \Phi} \left[ R_0 \left( \frac{z_v}{a} \right) B_{\theta a} \right]. \tag{B9}$$

Inverting to find $\frac{\partial V}{\partial \Phi}$

$$\frac{\partial V}{\partial \Phi} = -E_r \left( \frac{a}{R_0 z_v B_{\theta a}} \right). \tag{B10}$$

Substituting this back into Eq. (B8) and also substituting in our definition of $\nabla \Phi$ from Eq. (B5), we find

$$\mathbf{E} = E_r(z_v(\Phi)) \left\{ \left[ \frac{R}{R_0} \frac{a}{z_v(\Phi)} \frac{B_z}{B_{\theta a}} + \frac{(R - R_0)}{z_v(\Phi)} \right] \hat{R} + \left[ \frac{z}{z_v(\Phi)} \right] \hat{z} \right\}. \tag{B11}$$

### 1. Outer flux surface

We define our outer flux surface by $z_v = a$. However, when calculating banana widths, we generally start by considering a particle at $z = 0$. For small $\frac{a}{R_0} \frac{B_z}{B_{\theta a}}$, the minor radius *as measured from the flux axis* $r_F = R - R_v$ at $z = 0$ is

$$r_F = \frac{a}{\sqrt{1 + \frac{a}{R_0} \frac{B_z}{B_{\theta a}}}}. \tag{B12}$$

Initializing particles at this radius allow us to compare results between different $B_z$ values.

## APPENDIX C: COLD PARTICLE TRAPPING FOR NON-EQUIPOTENTIAL FLUX SURFACES

The conserved quantities along the particle orbit are

$$\epsilon = \frac{1}{2} m(v_\perp^2 + v_\parallel^2) + qV, \tag{C1}$$

$$\mu = \frac{1}{2} m \frac{v_\perp^2}{|B|}, \tag{C2}$$

$$p_\phi = mRv_\phi + qRA_\phi. \tag{C3}$$

For the following discussion, we will assume that $E_r$ is constant and $B_\theta = B_{\theta a} \left( \frac{r}{a} \right)$ at $R = R_0$.

We first note that

$$v_\phi = v_\parallel \left( \frac{B_\phi(R)}{|B|} \right) \tag{C4}$$

and of course

$$|B| = \left( B_\phi^2 + B_z^2 + B_R^2 \right)^{1/2}, \tag{C5}$$

$$= \left( B_\phi(R)^2 + B_z^2 + B_\theta(R, r)^2 - 2B_z B_\theta(r, R) \cos \theta \right)^{1/2}, \tag{C6}$$

where

$$B_\phi(R) = \frac{R_0}{R} B_{\phi 0}, \tag{C7}$$

$$B_\theta(R, r) = \frac{R_0}{R} \left( \frac{r}{a} \right) B_{\theta a}, \tag{C8}$$

$$\cos \theta = \frac{R - R_0}{r}. \tag{C9}$$

Now, our potential is given by

$$V(r) = -rE_r. \tag{C10}$$

Our vector potential is given by

$$A_\phi(R, r) = \frac{1}{2} RB_z + \frac{1}{2} \frac{R_0}{R} \frac{r^2}{a} B_{\theta a}. \tag{C11}$$

Our orbit constraint equation is then given by

$$0 = \frac{1}{2} m \left( \frac{p_\phi - qRA_\phi(R, r)}{mR} \right)^2 \left( \frac{|B(R, r)|}{B_{\phi 0}} \frac{R}{R_0} \right)^2$$
$$+ \mu|B(R, r)| + qV(r) - \epsilon, \tag{C12}$$

where the COMs are calculated from the initial conditions.

With our COMs in hand, we now turn to the question of electron trapping. Consider Eq. (C12) with $v_{\perp i}, v_{\parallel i} = 0$. Also, take $|B| \approx B_\phi$, $R_0/R \approx 1$. Then, substituting Eqs. (C10) and (C11), we find

$$0 = \frac{1}{2}\frac{q^2}{m}\left(\frac{1}{2}\frac{B_z}{R}\left(R_i^2 - R^2\right) + \frac{1}{2}\frac{B_{\theta a}}{a}\left(r_i^2 - r^2\right)\right)^2 - qE_r(r - r_i). \tag{C13}$$

Now, take

$$\Delta \equiv R - R_i, \tag{C14}$$

$$\bar{R} \equiv \frac{1}{2}(R + R_i), \tag{C15}$$

$$\delta \equiv r - r_i, \tag{C16}$$

$$\bar{r} \equiv \frac{1}{2}(r + r_i). \tag{C17}$$

Then, by noting $R_i^2 - R^2 = (R_i + R)(R_i - R) = -2\bar{R}\Delta$, we can rewrite the above equation as

$$0 = \frac{1}{2}\frac{q^2}{m}\left(B_z\frac{\bar{R}}{R}\Delta + B_{\theta a}\frac{\bar{r}}{a}\delta\right)^2 - qE_r\delta, \tag{C18}$$

$$\approx \frac{1}{2}\frac{q}{m}\left(B_z\Delta + B_{\theta a}\frac{\bar{r}}{a}\delta\right)^2 - E_r\delta. \tag{C19}$$

Now, we will consider the case where $z = 0$ so that $R = R_0 \pm r$. For an untrapped orbit which starts at $R_i < R_0$, we must have $R > R_0$ at the next midplane crossing, and so

$$\Delta = R - R_i = (R_0 + r) - (R_0 - r_i) = r + r_i = 2\bar{r}. \tag{C20}$$

Substituting this into Eq. (C19) and expanding the square, we find

$$0 = 4B_z^2\bar{r}^2 + \left(4B_zB_{\theta a}\left(\frac{\bar{r}^2}{a}\right) - \frac{2m}{q}E_r\right)\delta + B_{\theta a}^2\left(\frac{\bar{r}}{a}\right)^2\delta^2. \tag{C21}$$

For the moment, assume $\delta \ll r_i$ so that $\bar{r} \approx r_i$. Then, we have a simple quadratic equation, the solution to which is

$$\delta = -\frac{B}{2A}\left(1 - \sqrt{1 - \frac{4AC}{B^2}}\right), \tag{C22}$$

where

$$A = B_{\theta a}^2\left(\frac{r_i}{a}\right)^2, \tag{C23}$$

$$B = 4B_zB_{\theta a}\left(\frac{r_i^2}{a}\right) - \frac{2m}{q}E_r, \tag{C24}$$

$$C = 4B_z^2r_i^2. \tag{C25}$$

Because $4AC/B^2 > 0$ always, the magnitude of $\delta$ will go as $C/B \le aB_z/B_{\theta a}$. So, as long as $B_z/B_{\theta a} \ll r_i/a$, then $\delta \ll r_i$, and everything is consistent.

Because $A$ and $C$ are strictly positive, this equation will only have a real solution when $4AC/B^2 < 1$, i.e., when

$$\left(4B_zB_{\theta a}\left(\frac{\bar{r}^2}{a}\right) - \frac{2m}{q}E_r\right)^2 > \left(4B_zB_{\theta a}\frac{\bar{r}^2}{a}\right)^2. \tag{C26}$$

Now, force balance requires $B_zB_{\theta a} > 0$. Thus, we can see that when $qE_r > 0$, as is the case for electrons in a negatively biased WDRT, the LHS is strictly smaller until the second term is twice as large as the first term. The minimum electric field to satisfy this condition is

$$|E_r| > 4\frac{|q|}{m}B_zB_{\theta a}\frac{r_i^2}{a}. \tag{C27}$$

This is our first passing orbit condition.

To find the second condition, consider the limit $B_{\theta a} \to 0$. Now, we can no longer take $\delta \ll r_i$; instead, $\bar{r} = \delta/2 + r_i$. Thus,

$$\delta E_r \approx \frac{2q}{m}B_z^2\bar{r}^2, \tag{C28}$$

$$\approx \frac{2q}{m}B_z^2\left(\delta^2/4 + \delta r_i + r_i^2\right). \tag{C29}$$

So

$$0 = r_i^2 + \left(r_i - \frac{m}{2qB_z^2}E_r\right)\delta + \frac{1}{4}\delta^2. \tag{C30}$$

Similarly to before, the answer is simply quadratic, given by

$$\delta = -\frac{B}{2A}\left(1 - \sqrt{1 - \frac{4AC}{B^2}}\right), \tag{C31}$$

where now

$$A = 1/4, \tag{C32}$$

$$B = r_i - \frac{m}{2qB_z^2}E_r, \tag{C33}$$

$$C = r_i^2. \tag{C34}$$

So, for a real solution to exist, we must have $4AC/B^2 < 0$, i.e., (for $qE_r > 0$)

$$|E_r| > 4\frac{|q|}{m}B_z^2r_i. \tag{C35}$$

Thus, our two conditions on $E_r$ are

$$|E_r| > \begin{cases} 4\dfrac{|q|}{m}B_zB_{\theta a}\dfrac{r_i^2}{a} & \text{if } B_z/B_{\theta a} \ll r_i/a \\ 4\dfrac{|q|}{m}B_z^2r_i & \text{if } B_z/B_{\theta a} \gg r_i/a. \end{cases} \tag{C36}$$

To test these predictions, we ran single-particle simulations (Boris scheme) for fixed values of all parameters besides $E_r$; if the orbit was trapped, $|E_r|$ was increased, while if it was untrapped, it was decreased. Once both trapped and untrapped orbits were identified, this process became a binary search for the minimum $|E_r|$ required for orbit untrapping.

The comparison of these simulations with Eq. (C36) is shown in Fig. 7. Each theoretical prediction agrees well with the simulation in its regime of applicability.
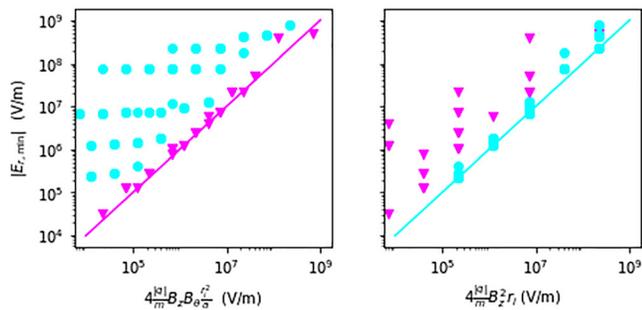
FIG. 7. Comparison of theoretical minimum $|E_r|$ for an untrapped orbit with the minimum magnitude required in single-particle simulations. Magenta triangles represent $B_z/B_{\theta a} < r_i/a$, while cyan circles represent $B_z/B_{\theta a} > r_i/a$. The theoretical value in each regime of Eq. (C36) accurately describes the trapping condition.

[1]G. Janes, R. Levy, H. Bethe, and B. Feld, "New type of accelerator for heavy ions," Phys. Rev. **145**, 925 (1966).

[2]K. Avinash, "On toroidal equilibrium of non-neutral plasma," Phys. Fluids B: Plasma Phys. **3**, 3226–3231 (1991).

[3]P. Zaveri, P. John, K. Avinash, and P. Kaw, "Low-aspect-ratio toroidal equilibria of electron clouds," Phys. Rev. Lett. **68**, 3295 (1992).

[4]T. H. Stix, "Toroidal fusion plasma with powerful negative bias," Phys. Rev. Lett. **24**, 135 (1970).

[5]T. H. Stix, "Some toroidal equilibria for plasma under magnetoelectric confinement," Phys. Fluids **14**, 692–701 (1971).

[6]T. H. Stix, "Stability of a cold plasma under magnetoelectric confinement," Phys. Fluids **14**, 702–712 (1971).

[7]R. Taylor, J.-L. Gauvreau, M. Gilmore, P.-A. Gourdain, D. LaFonteese, and L. Schmitz, "Initial plasma results from the electric tokamak," Nucl. Fusion **42**, 46 (2002).

[8]I. Nascimento, Y. K. Kuznetsov, J. Severo, A. Fonseca, A. Elfimov, V. Bellintani, M. Machida, M. Heller, R. Galvão, E. Sanada *et al.*, "Plasma confinement using biased electrode in the TCABR tokamak," Nucl. Fusion **45**, 796 (2005).

[9]R. Taylor, T. Carter, J.-L. Gauvreau, P.-A. Gourdain, A. Grossman, D. LaFonteese, D. Pace, L. Schmitz, A. White, and T. Yates, "Particle pinch mitigated by radial currents in the electric tokamak," Nucl. Fusion **45**, 1634 (2005).

[10]J. Rax, R. Gueroult, and N. Fisch, "Efficiency of wave-driven rigid body rotation toroidal confinement," Phys. Plasmas **24**, 032504 (2017).

[11]N. J. Fisch and J.-M. Rax, "Interaction of energetic alpha particles with intense lower hybrid waves," Phys. Rev. Lett. **69**, 612 (1992).

[12]A. J. Fetterman and N. J. Fisch, "α channeling in a rotating plasma," Phys. Rev. Lett. **101**, 205003 (2008).

[13]N. J. Fisch, "Confining a tokamak plasma with rf-driven currents," Phys. Rev. Lett. **41**, 873 (1978).

[14]N. J. Fisch, "Theory of current drive in plasmas," Rev. Mod. Phys. **59**, 175 (1987).

[15]J. Wesson and D. Campbell, *Tokamaks* (Oxford University Press, 2011), Vol. 149.

[16]J. M. Rax, *Physique Des Tokamaks* (Editions de l'Ecole Polytechnique, Paris, 2011).

[17]V. S. Tsypin, R. M. O. Galvao, I. C. Nascimento, M. Tendler, J. H. F. Severo, and L. F. Ruchko, "Role of trapped and circulating particles in inducing current drive and radial electric field by Alfven waves in tokamaks," J. Plasma Phys. **67**, 301 (2002).

[18]K. Wong and C. Cheng, "Orbit effects on impurity transport in a rotating tokamak plasma," Phys. Fluids B: Plasma Phys. **1**, 545–554 (1989).

[19]J. P. Boris, "Relativistic plasma simulation-optimization of a hybrid code," in *Proceedings of the Fourth Conference on the Numerical Simulation of Plasmas* (Naval Res. Lab, Washington, DC, 1970), pp. 3–67.

[20]J.-L. Vay, "Simulation of beams or plasmas crossing at relativistic velocity," Phys. Plasmas **15**, 056701 (2008).